UT-S&E-LASER/DEC

Task Title: STUDIES ON PYROMETER MEASUREMENTS FOR FAST AND INHOMOGENEOUS LASER HEATING

INTRODUCTION

High repetition rate laser ablation (LA) may be effective for cleaning and detritiation of internal walls of D-T thermonuclear tokamak installations, like ITER [1-7]. The modelling of laser heating and LA of graphite samples from different tokamaks is important to optimise laser detritiation of graphite surfaces and to characterise carbon deposits (thickness, thermal and optical properties, adhesion and heat contact with graphite substrate, etc). Pyrometer measurements can be applied to determine layer properties by theoretical fit of experimental heating temperatures. Nevertheless, some parameters of commercial pyrometers (microsecond response time, limited temperature range with top and bottom temperatures) impose certain limitations on pyrometer measurements. For graphite and metal surfaces at laser heating by nanosecond or shorter laser pulses, the surface temperature may differ from the one on the pyrometer output due to averaging on the microsecond response time. A similar problem occurs if the laser beam is inhomogeneous (tightly-focused Gaussian laser beam) or the surface incorporates highly absorptive micro-inclusions.

2006 ACTIVITIES

FAST AND INHOMOGENEOUS LASER HEATING

Studies on pyrometer features are required to obtain reliable results on the surface temperature for inhomogeneous and fast laser heating. Expression for pyrometer output photocurrent is

$$I_{eff}(t) = \int_{-\infty}^{t} F_T(t-t') I_{photo}(t') dt' ,$$ where

$$I_{photo}(t) = A(\omega) \frac{\omega^2 \Delta\omega}{4\pi^2 c^2} \int_0^{2\pi} \int_0^{+\infty} \frac{F_S(r) \cdot r\, dr d\varphi}{\exp\left(\hbar\omega / T(t, \vec{r})\right) - 1},$$

with $F_T(\tau)$ – pyrometer influence function for time averaging of the pyrometer photocurrent $I_{photo}(t)$, $F_S(r)$ - space-geometrical factor. In the expression for $I_{photo}(t)$, ω and $\Delta\omega$ are pyrometer working and band frequencies, $A(\omega)$ - surface absorptivity on frequency ω, $T(t, r)$ - local surface temperature at the moment t and in a surface point r from the center of the pyrometer light collector axis. The current $I_{eff}(t)$ is the result of averaging the photo-current $I_{photo}(t)$ created in the pyrometer photo-detector with the influence function $F_T(\tau)$, which is associated with the finite response time of the pyrometer. This function should satisfy the general condition: $\int_0^{+\infty} F_T(\tau) d\tau = 1$.

Application of the factor $\Delta\omega = \omega_{max} - \omega_{min}$ (ω_{min} and ω_{max} are the limits of the pyrometer frequency band) is justified by a high ratio of $\hbar\omega_{min} / T$ that allows to apply approximation $\omega \cong \omega_{min.}$. Thus**,** here, single-colour pyrometer measurements are considered. We suppose circular symmetry of the pyrometer light collector.

Function $F_S(r) = \int \cos\theta \, d\Omega$ is the space geometrical factor related with the pyrometer fiber diameter and numerical aperture, and its location with respect to the surface. The integration is provided over the solid angle determined by the position of the lens with respect to the point r. With the good accuracy for our measurements, we can assume $F_S(r) = 0$ at $r > r_0$ and $F_S(r) = F_0 = \text{Const}$ at $r < r_{0.}$ In our experiments, r_0 = 500 - 700 μm **(**r_0 - radius of the light collection area on the surface). For Impac-Kleiber C-LWL infrared pyrometer applied in our experiments, the response time of RC-circuit (τ_o) is in a microsecond range. For electronic RC-circuit, the influence function is exponential, that is, $F_T(\tau) = \tau_0^{-1} \exp(-\tau / \tau_0)$. The pyrometer influence function should be known if the time of the temperature change during the measurements is shorter than one microsecond. The influence function can approximately be determined from the temperature measurements. From the mathematical point of view, the influence function $F_T(\tau)$ presents the pyrometer electric current response on the pyrometer output, if the received photocurrent is a very short pulse (like the Dirac $\delta(t)$-function), that is, if $I_{photo}(t) \sim \delta(t)$.

Thus, $I_{eff}(t) \sim F_T(t)$. Based on the graphite temperature measurements with 100 ns laser pulses, we can conclude that $F_T(\tau)$ - function of our pyrometer can roughly be approximated by $F_T(\tau) \sim \tau^n \exp(-\tau / \tau_0)$.

The plot of $F_T(\tau)$ with $n = 2$ and τ_0 = 1.785 μs is shown in figure 1(a). Its integral over τ from 0 up to time t is presented in figure 1 (b).

For this function, $\int_0^{t=15\mu s} F_T(\tau) d\tau = 0.99$, which corresponds to the reference data of our pyrometer.

The integrated function of figure 1(b**)** determines the pyrometer response to a step-wise signal, when $I_{photo}(t) = 0$ at $t < 0$ and $I_{photo}(t) = I_0 = \text{Const}$ at $t > 0$.

The pyrometer output temperature $T_{exp}(t)$ can be related with the effective current $I_{eff}(t)$ as:

$$I_{eff}(t) = \frac{\omega^2 \Delta\omega}{4\pi^2 c^2} \frac{A_{emph}}{\exp\left(\hbar\omega / T_{exp}(t)\right) - 1} \int_0^{+\infty} F_S(r) \cdot 2\pi r dr$$

where A_{emph} - empirical surface emissivity.

Taking into account $F_S(r)$ function properties, the relation between the temperature $T_{exp}(t)$ given by the pyrometer and the real surface temperature $T(t, r)$ can be expressed as:

$$T_{exp}(t) = \frac{\hbar\omega}{\ln\left(1 + \left[\frac{A(\omega)}{A_{emp}}\int_0^{+\infty}\frac{F_T(\tau)}{\pi r_0^2}\left\{\int_0^{2\pi}\int_0^{r_0}\frac{r dr d\varphi}{\exp\left(\hbar\omega/T(t-\tau,\vec{r})\right)-1}\right\}d\tau\right]^{-1}\right)}$$

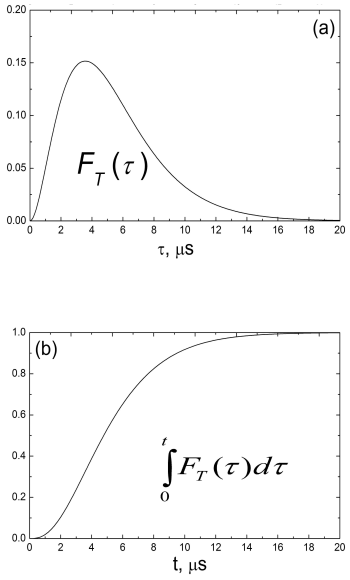

Figure 1: The influence function $F_T(\tau) \sim \tau^n \exp(-\tau/\tau_0)$ *of the pyrometer - Panel (a); its integral over* τ *from 0 up to t - Panel (b). Here, n = 2 and* $\tau 0 = 1.785\ \mu s$

FAST LASER HEATING

For nanosecond laser heating, we assume that the radius of homogeneous laser spot on the surface is higher than the radius r_0 of the pyrometer photo-collector. For homogeneous temperature distribution, the above expression for $T_{exp}(t)$ can be simplified:

$$T_{exp}(t) = \frac{\hbar\omega}{\ln\left(1 + \left[\frac{A(\omega)}{A_{emp}}\int_0^{+\infty}\frac{F_T(\tau)}{\exp\left(\hbar\omega/T(t-\tau)\right)-1}d\tau\right]^{-1}\right)}.$$

Empirical emissivity A_{emp} for graphite is assumed to be close to the actual one: $A_{emp} \cong 0.9 = A(\omega)$.
The theoretical temperature profile obtained with the laser heating model and the experimental one [3-7] for the same laser and medium parameters are presented in figure 2.
In expression for $T_{exp}(t)$, the pyrometer maximal working wavelength is $\lambda_{max} = 2\pi c/\omega_{min} = 2.2$ μm (c - light speed) that is in accordance with the pyrometer 1.8 – 2.2 μm spectral sensitivity range. On figure 2, blue curves present the experimental temperatures for heating of the backside surface of Tore Supra graphite sample (without deposited carbon layer and without any preliminary laser processing) by 100 ns laser pulses [5]. Black curves of figure 2 present theoretical temperatures obtained with the laser heating model. Theoretical data of panel 2(a) do not consider the upper temperature limit (2600 K) that can be registered by the pyrometer. The averaged theoretical results of panel 2(b) take this limitation into account.
The results of figures 2(a) and 2(b) are very close. On figures 2(a) and 2(b), the theoretical peak temperature is much higher than the experimental one from the pyrometer output. The width of the experimental temperature peaks is much higher than 100 ns (laser pulse duration). The experimental maximum temperature is reached at some microseconds, that is, also much higher than the laser pulse duration. The actual maximum temperature could be supposed close to the graphite sublimation temperature (about 4300 K). But the experimental maximal temperature measured by the pyrometer is much lower due to microsecond response time of the pyrometer.
On figures 2(a) and (b), the red curves present the averaged theoretical results. They are in a good qualitative (and even semi-quantitative) agreement with the experimental results.

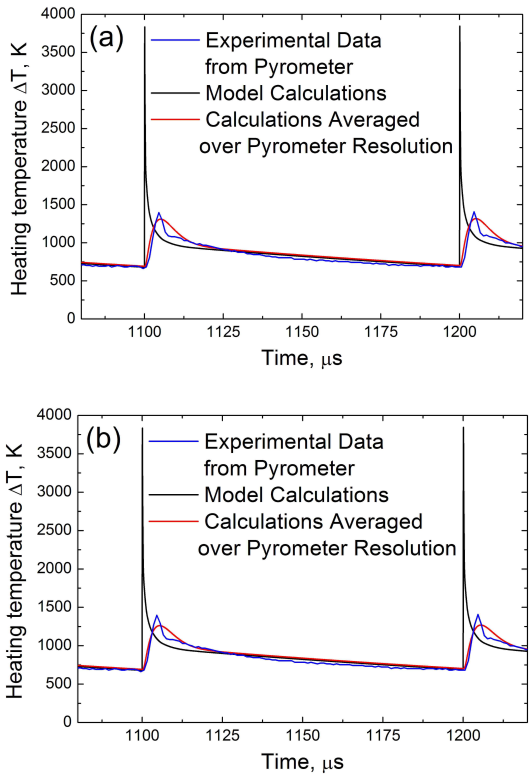

Figure 2: Theoretical results (red curves) on laser heating by ns laser pulses averaged according to expression for $T_{exp}(t)$ *with the smoothed spread influence function of Figure 1 and corresponding experimental results (blue curves). Theoretical data of panel 2(a) do not take into account the pyrometer upper temperature limit (2600 K). Panel 2(b) presents the averaged calculations with this pyrometer limitation in mind*

INHOMOGENEOUS LASER HEATING

For the pyrometer measurements of surface laser heating by a tightly-focused laser beam, the radial distribution of the laser intensity should be taken into account. The case $r_L < r_0$ is considered. Here, r_L - the width of the Gaussian laser intensity distribution on the surface $I(r) = I_0 \exp(-r^2/r_L^2)$. If the laser heating time is short enough, the radial distribution of the surface temperature

can also be considered as Gaussian, that is, $T(r) = T_{\max} \exp(-r^2 / r_L^2)$ with the same width. For 0.2-, 2- and 20-millisecond laser pulses with r_L = 200 μm, the calculated temperature radial distributions on the graphite surface are presented on figure 3. The temperature distribution is Gaussian with the width $r_T \approx r_L$ = 200 μm for laser pulse durations < 200 μs. This time duration is significantly long if compared with the pyrometer response time.

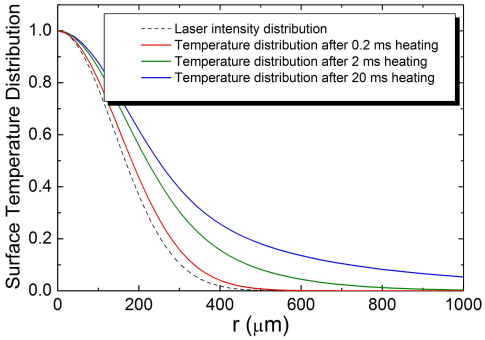

Figure 3: The surface temperature radial distribution at laser heating by the Gaussian laser beam with r0 = 200 μm and different pulse durations

For microsecond laser pulses and tightly-focused Gaussian laser beam, expression for the experimental temperature on the pyrometer output can be reduced to:

$$T_{exp} = \frac{\hbar\omega}{\ln\left(1 + \left[\frac{A(\omega)}{A_{emp}} \int_0^1 dx \left\{\exp\left(\frac{\hbar\omega}{T_{\max}} \exp\left(x \frac{r_0^2}{r_L^2}\right)\right) - 1\right\}^{-1}\right]^{-1}\right)}$$

Microsecond pulse durations are considered to avoid the problem of time averaging. Assuming that A_{emp} = A(ω), the dependences of the pyrometer temperature as a function of the actual temperature in the laser spot centre on the surface are presented in figures 4 (a, b, c), for pyrometers with working wavelengths (λ_{pyr} maximal) of 2.2 μm, 1.0 μm and 0.5 μm, respectively. The temperature measured by pyrometer differs from the actual temperature in the laser spot centre. The higher the temperature is, the more evident the difference between the actual temperature and the one measured by the pyrometer. If the width of the Gaussian laser beam is known, it is possible with the curves of figure 4(a) to restore the actual surface temperature from the experimental one. The difference between the actual and the measured temperature is reduced with the working wavelength decrease. The measured temperature of panel 4(c) is close to the actual one for the temperatures up to 1000 K. Thus, the lower working wavelengths should be considered preferable for pyrometer temperature measurements of laser heating with a tightly-focused Gaussian laser beam. From the panels of figure 4, the relative errors of the temperature measurements (within the above parameter range) do not exceed 10% even for a pyrometer with a longer 2.2 μm working wavelength. Thus, the appropriate choice of the pyrometer may ensure reliable measurements of laser heating temperature for surface characterization.

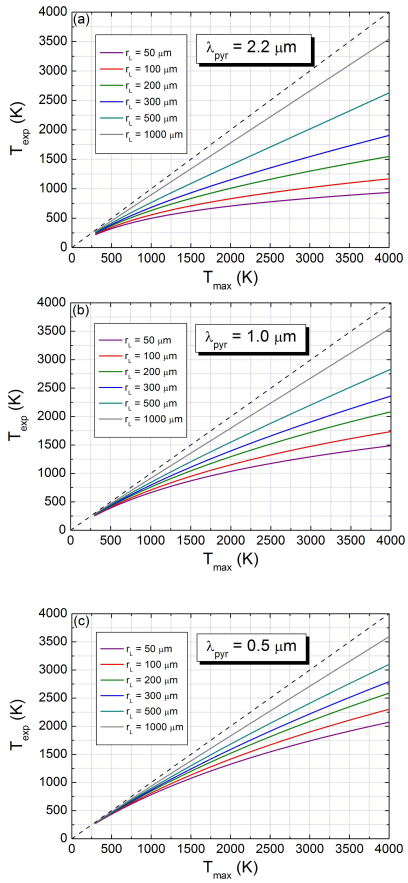

Figure 4: The experimental temperature T_{exp} on the pyrometer output as a function of the actual temperature T_{max} in the centre of the Gaussian laser beam on the surface for different widths (r_L) of the Gaussian laser beam. Panels (a), (b) and (c) correspond to 2.2, 1.0 and 0.5 μm wavelengths λ_{pyr}, respectively. The pyrometer collected area radius is 500 μm.

For graphite laser heating, the medium should not be regarded as completely homogeneous. Small-localized centres and background (matrix) of different absorption may be found on the surface. The inhomogeneity of graphite tiles can be attributed to graphite porosity and internal random microstructure or deposited carbon layer inhomogeneity. Some isolated local absorption centres can be found in the deposited layer. During laser pulse heating, these centres may predominantly contribute to the heating temperature measured by pyrometer.

The temperature will tend to homogenise due to thermal conductivity and heat flow from the local centres to the matrix. For nanosecond laser pulses, this process is much slower on the laser pulse scale. It is defined by thermal diffusivity of the matrix. In the heat equations, the laser heating source term $Q_i(\mathbf{r})$ corresponding to a single local centre *i* in position $\mathbf{r}_i$ on the surface (or inside the medium) can be written as: $Q_i(\vec{r}) = I(\vec{r})\sigma_{abs}\delta(\vec{r} - \vec{r}_i)$, where $I(\mathbf{r})$ - local laser intensity on the surface or inside the medium (in the local heating centre $\mathbf{r}_i$), σ_{abs} - its absorption cross-section depending on centre index *i*. A higher temperature of the local heating centre than the one of the matrix is associated with the high absorption cross-section σ_{abs} of the centres. The local heating centres are distributed over the medium with the volume density n_c. Their contribution to the heating temperature is determined by absorption

coefficient $n_c \cdot \sigma_{abs}$ of the local centres. The matrix (background) absorption coefficient α should be compared with the one of the local centres. If $\alpha >> n_c \cdot \sigma_{abs}$, the effect of the local centres is negligible. If $\alpha << n_c \cdot \sigma_{abs}$, the temperature of the local centres can be higher than the one of the matrix during nanosecond laser pulse heating. The mean distance between the local heating centres and thermal diffusion length in the background (matrix) should also be considered. If $n_c^{-1/3} << \sqrt{Dt_p}$ (D - thermal diffusion coefficient of the matrix and t_p – laser pulse duration), the temperature homogenization will take place on the scale of the laser pulse duration. In this case, the mean heating temperature is defined by the mean absorption coefficient of the matrix with the local centres distributed with concentration n_c. If $n_c^{-1/3} >> \sqrt{Dt_p}$, the temperature homogenization will occur just after laser pulse interaction with surface. Thus, the contribution of the local absorption centres in the measured temperature is important if:

$$\alpha << n_c \cdot \sigma_{abs},$$
$$n_c^{-1/3} >> \sqrt{Dt_p}\ .$$

The last inequality implies that the typical dimension of the absorption center is smaller than the heat diffusion length. Otherwise, the medium may be considered homogenous.

CONCLUSIONS

The previously developed model for homogeneous laser heating [3], [4], [5], [7] was extended to study fast and/or inhomogeneous surface heating. The relation between the experimental temperature T_{exp} *(t)* in the pyrometer output and the actual temperature *T (t, r)* of the surface was established. This relation was applied to analyse particular features of laser heating by nanosecond laser pulses in combination with on-line pyrometer measurements of the surface temperature. Pyrometer measurements for inhomogeneous heating by a tightly-focused Gaussian laser beam were analysed. For the Gaussian laser intensity distribution, the temperature measured by the pyrometer differed from the actual temperature in the laser spot centre. It was found that the higher the temperature, the more pronounced this difference was. With the known width of the Gaussian laser intensity distribution, it was possible to restore the actual surface temperature from the experimental one obtained by the pyrometer. Inhomogeneous laser heating resulting from highly absorbing centres on the surface heated much higher than the background was under investigation. The parameter range (absorption coefficient and density) was determined for absorption centres which contributed significantly to the measured temperature. Certain pyrometer parameters (microsecond response time and limited temperature range) were under special consideration. It was demonstrated that the actual and theoretical peak temperature can be much higher than the experimental one in the pyrometer output. The widths of the experimental temperature peaks were about some microseconds, that is, much higher than the laser pulse duration. The theoretical data were compared with the experimental pyrometer measurements. They were found in a good agreement.

REPORTS AND PUBLICATIONS

[1] A. Semerok J.-M. Weulersse, F. Brygo, C. Lascoutouna, C. Hubert, F. Le Guern, M. Tabarant, Studies on graphite surfaces detritiation by pulsed repetition rate nanosecond lasers, CEA report, NT DPC/SCP/04-076-A, 2004, pp.1 - 39

[2] A. Semerok, J-M. Weulersse, F. Brygo, D. Farcage, C. Hubert, C. Lascoutouna, M. Géléoc, P. Wodling, H. Long, F. Champonnois, G. Brunel, G. Vimond, E. Lizon, V. Dauvois, V. Delanne, C. Grisolia, S. Fomichev, M. Hashida, Studies on TOKAMAK wall surfaces decontamination by pulsed repetition rate lasers, CEA report, NT DPC/SCP/05–111–A, 2005, pp.1 – 50

[3] S.V. Fomichev, A. Semerok, J.M. Weulersse, F. Brygo, Modelling of complex surface heating by continuous and pulsed lasers, CEA report, NT DPC/SCP/05–109–A, 2005, pp.1-76

[4] A. Semerok, S.V. Fomichev, F. Brygo, J.-M. Weulersse, P.-Y. Thro, C. Grisolia, Surface heating by pulsed repetition rate nanosecond lasers, Invited presentation on the 4th International Symposium “LASER TECHNOLOGIES AND LASERS”, October 8- 11, 2005, Plovdiv, Bulgaria, paper in the LTL Symposium Proceedings, April, 2006, pp. 76-83, ISSN 1312-0638

[5] A. Semerok, S. V. Fomichev, F. Brygo, P.-Y. Thro, Laser heating of complex graphite surfaces by high repetition rate nanosecond pulses (comparative modelling and experimental studies), CEA report, NT DPC/SCP/06–170–A, 2006, pp.1 – 36

[6] A. Semerok, P.-Y. Thro , J.-M. Weulersse, S.V. Fomichev, F. Brygo, C. Grisolia, V. Philipps, P. Coad and JET EFDA contributors, Laser Methods Development for In-situ ITER Walls Detritiation and Deposition Layers Characterisation, Invited presentation on the 6th Fusion Energy Conference (FEC), 16–21 October 2006, Chengdu, China

[7] A. Semerok., S.V. Fomichev, J.-M. Weulersse, F. Brygo, P.-Y. Thro, Heating and ablation of tokamak graphite by pulsed nanosecond Nd-YAG lasers, Journal of Applied Physics, paper accepted for publication in 2007

[8] A. Semerok. and S.V. Fomichev, Studies on pyrometer measurements for fast and inhomogeneous laser heating, CEA report, NT DPC / SCP/06-212- A, 2006, pp.1 – 19

TASK LEADER

Alexandre SEMEROK

DEN/DPC/SCP/LILM
CEA-Saclay
F-91191 Gif-sur-Yvette Cedex

Tel. : 33 1 69 08 65 57
Fax : 33 1 69 08 78 84

e-mail : alexandre.semerok@cea.fr

UT-S&E-LiPbwater

Task Title: CONSEQUENCES OF A Pb/Li – WATER INTERACTION IN THE ITER VACUUM VESSEL

INTRODUCTION

In the framework of the Safety Analysis of the ITER reactor, the consequences of a common failure of the Test Blanket Module (TBM) and a few blankets dedicated to the water-cooling are investigated. In such conditions, it would result in an interaction between the metal Pb/Li liquid coming from the TBM and water in the vacuum vessel. The contact between these two fluids at relatively high temperature could lead to a thermal interaction followed by an exothermic chemical reaction with a large energy release. The water would vaporize and thus pressurize the vacuum vessel, designed to withstand a maximum pressure of 2 bar. If such pressure was reached, the integrity of the vessel could be challenged.
This specification study consists in assessing the maximum pressure reached in the vacuum vessel by a thermodynamic approach.
For 2007, it will be proposed to continue this analysis by a modeling with the SIMMER-III code, taking into account the kinetics aspects of the mixing. The initial phase after the contact of the two liquids, which is subjected to the apparition of pressure peaks, will be particularly investigated.

2006 ACTIVITIES

The objective of the 2006 work was to analyze the thermal interaction and to propose a modeling to simulate it.

STATUS ON PREVIOUS STUDIES
In 1999, the consequences of the Pb/Li – water interaction were investigated by Utschig and Corradini in the framework of the initial ITER project [1]. Two different computer codes LINT and MELCOR were adapted for this evaluation in non-equilibrium conditions. At that time, the TBM was only cooled by water so that the risk of a Pb/Li and water interaction was much bigger than today. Furthermore, the vessel size was bigger, temperature and pressure were also different. The thermal interaction and the chemical reaction were modeled at that time.
In this analysis, the vessel failure was assumed to occur if pressure exceeds 5 bar.

The results are as follows:
- assuming a Pb/Li leak into water filled vessel, no failure occurs in a vessel already filled with water since the pressure is limited the maximum Pb/Li pressure, which is always below the design pressure,
- assuming a water leak into a pre-existing lithium vessel and no break of the rupture disk between the vacuum vessel and the relieve tank, a vessel failure is assessed within a few minutes. The Pb/Li will rapidly disappear but the vessel pressure will continue to increase as long as water is injected. Temperatures up to 3000 K were calculated in transient situation and adiabatic condition. Heat transfer out of the vessel will however limit these temperatures. Without any Li/Pb in the vessel, a mass of 9300 kg water was predicted by calculation, which decreases to 1500 kg if 1000 kg of Li/Pb was already in the vessel.

These results must be updated in order to take into account the modifications made on the ITER reactor design, in particular the replacement of the water cooling system by a helium cooling one and the decrease of the free vacuum volume (1350 m^3 instead of 3800 m^3). The use of the computer code SIMMER-III, already validated for this kind of interactions, is chosen for the modeling [2].

In the past, the BLAST and LIFUS programs were performed by ISPRA [3] to evaluate the Pb/Li – water interaction. The SIMMER-III calculations produced good results on these tests [4] & [5]. The modeling developed at that time will be adapted for the present study. The kinetics aspects of the mixing between the two fluids will be taken into account and the thermal interaction will be determined.

Chemical reaction
It is also useful to present the chemical reaction between water and Pb/Li.
Two situations could occur: a small leakage or a large leakage. In both cases, the chemical reaction that takes place is [1]:

Reaction in the presence of excess water:

$$2Li + 2H_2O \rightarrow 2LiOH + H_2 \quad \Delta H = -29\,MJ/kg - Li\ at\ 25°C$$

Reaction in the presence of excess lithium:

$$2Li + H_2O \rightarrow Li_2O + H_2 \quad \Delta H = -22\,MJ/kg - Li\ at\ 25°C$$

These chemical reactions are exothermic, leading to a very large pressure increase in the module blanket, exceeding the design pressure.

THE THERMO-DYNAMICAL STUDY
Prior to a computer modeling, a global evaluation of the energy release is proposed for two situations (water or Pb/Li leak).

The vessel pressurization without helium
The Pb/Li liquid metal is initially pressurized to 2 bar and at a temperature of 550 °C, the water being at 30 bar and 150°C.

The water vaporization

In order to give an order of magnitude of the maximum pressure reached, a first calculation is performed. A Pb/Li leak and a water leak will be respectively estimated.

The thermo-dynamical characteristics of the water are summarized in table 1.

Table 1: Properties of the water (1, 2, 5 and 30 bar)

	Water properties			
Pressure	1 bar	2 bar	5 bar	30 bar
Melting latent heat	$2.259 \cdot 10^6$ J/kg	$2.204 \cdot 10^6$ J/kg	$2.111 \cdot 10^6$ J/kg	$1800 \cdot 10^6$ J/kg
Saturation temperature	99.09 °C	120°C	151 °C	233°C
	Water saturation pressure			
Water saturation pressure				
Temperature	100 °C	150 °C	550 °C Above the critical temperature (T=374 °C)	
Saturation pressure	1 bar	4.85 bar		

As shown by the water characteristics (Figure 1), the water will immediately vaporize as soon as it comes into the vacuum vessel since its pressure is largely under the saturation pressure.

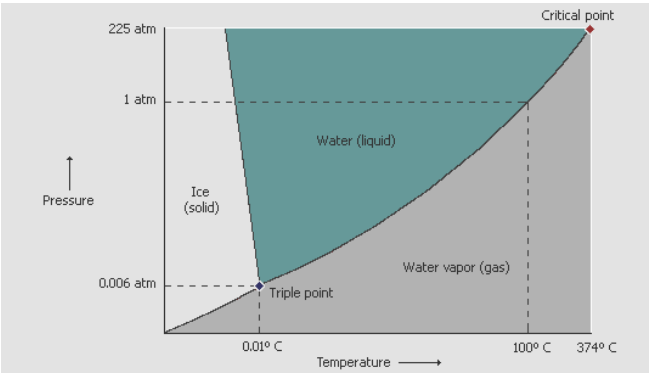

Figure 1: Water phase diagram

The initial characteristics of Pb/Li in the vacuum vessel are summarized in table 2:

Table 2: properties of Pb/Li

	Pb/Li
Pressure	2 bar
Volume	0.324 m^3
Mass	3235 kg
Initial temperature	550 °C
Liquid density	9984 kg/m^3
Steam density	190 J/K/kg
Melting temperature (2 bar)	235°C
Saturation temperature (2 bar)	978°C
Saturation pressure (550°C)	$1.235 \cdot 10^{-2}$ Pa
Specific heat	195 J/kg/K

It is to notice that Pb/Li remains in its liquid state between 235 and 978 °C under 2 bar.

Pb/Li leak

Initially, 1 m^3 of water at a temperature of 150°C is assumed to be present in the vacuum vessel. Pb/Li is also injected in its liquid state at a temperature of 550°C.

Due to thermal and chemical reaction with Pb/Li, water temperature will rapidly increase. As the total volume of the vacuum vessel is very large, the steam temperature corresponding to a pressure of 2 bar is also very high. Using the perfect gas law, the temperature necessary to pressurize the vessel is of the order of $T = \frac{P \cdot V}{n \cdot R} \approx 2 \cdot 10^6 K$, which is unrealistic, since the Pb/Li maximum temperature is only 550°C.

There is no risk of pressurization of the vessel if the water amount is limited to 1 m^3. The probability of pressure peaks is therefore also very low. This case will not be investigated in detail since the thermal energy between $1m^3$ water and 0.28 m^3 Pb/Li could not pressurize the vessel.

Previous analysis confirms that a vessel pressurization is unlikely in case of a lithium leak from the TBM into an initially water filled vessel. In addition, the low Lithium driving pressure results in limited risk of lithium leak [1].

Water leak

On the contrary, when water is injected into the vessel initially filled with a mass of 0.324 m^3 of Pb/Li at a temperature of 550°C, it will immediately vaporize.

A first conservative calculation, considering that the maximum vessel temperature is 550°C (the initial Pb/Li temperature), gives the steam mass necessary to reach a pressure of 2 bar in equilibrium condition. Using the perfect law gas, a water mass of 2000 kg, which is quite large but not unrealistic, is found.

If the final vessel temperature is only of 150°C, the water mass increases to 4000 kg.

Taking into account the heat transfer produced by the Pb/Li - water interaction and transferred to the vessel structure, the likely final temperature is comprised between 150 and 550°C, so that a risk of vessel failure could be feared.

In the previous work [1], the vessel failure was assumed to occur for a vessel design pressure of 5 bar. The water mass calculated by the LINT and MELCOR codes was 9700 kg in the absence of Pb/Li. This value is coherent with this approach. Indeed, if the vessel temperature is 150°C, the water mass necessary to reach failure is 4000*5/2=10000 kg.

Since water is pressurized as long as it is coming into the vessel, the vessel could fail even without any lithium interaction if there is no protection against over-pressure (rupture disk). The question is therefore to check whether this release valve is correctly dimensioned and works properly.

Although the water amount is quite large, additional calculations are proposed to study the transient effects. Indeed, pressure peaks are expected during the mixing phase that could damage the vessel structure.

2007 FORESEEN STUDY

These two studies were estimated on a thermodynamic viewpoint in 2006 in order to give a first evaluation on the consequences of the Pb/Li and water interaction. Only stationary conditions were studied.
The conditions to be considered for the 2007 modeling are based on the new ITER vacuum vessel geometry.
The reference case will be a water injection in a vacuum vessel already filled with Pb/Li. The thermal interaction and chemical reaction between them will be modeled.
It is proposed to perform this analysis by a refined modeling with the SIMMER code. The kinetics aspects of the mixing between the two liquids will be taken into account. The initial phase after the contact of the two fluids will be investigated and the results will be compared to the present ones.

CONCLUSIONS

The question raised by the consequences of a possible interaction between Pb/Li and water as well as a preliminary evaluation was done in 2006. The water mass necessary to endanger to vacuum vessel integrity was estimated. Although this approach leads to rapid results, it only corresponds to stationary conditions that take into account - neither the transient mixing process - nor the system geometry where the mixing takes place. Consequently, it is proposed to pursue this study in 2007 by a complete modeling of the control volume of the vacuum vessel. The thermal interaction would be more precisely estimated and the pressures on the vessel will be better calculated.

REFERENCES

[1] Computer Modeling for Lithium Safety in Fusion Systems: LINT and MELCORT.T Utschig and M.L Corradini (June 1999) Fusion Technology Institute University of Wisconsin

[2] SIMMER-III: a computer code for LMFR core disruptive accident analysis Version 2.H model summary and program description S. Kondo et al (November 2000) JNC TN9400 2001-002

[3] LIFUS 5 : experimental facility on PB-17Li alloy – water interaction to be build at ENEA Brasimone center – Technical specification G. Benamati and CO (March 1997)

REPORTS AND PUBLICATIONS

[4] “Recalculation of the LIFUS experiment with the 3D version of SIMMER” (interaction between lithium-lead and water)
T. Cadiou (February 2005)

[5] “modelling of the interaction between lithium-lead and water using the SIMMER-III code”
T. Cadiou (January 2004)

TASK LEADER

Thierry CADIOU

DEN/DER/SESI/LCSI
CEA-Cadarache
F-13108 Saint-Paul-lez-Durance Cedex

Tel. : 33 4 42 25 66 17
Fax : 33 4 42 25 71 87

e-mail : thierry.cadiou@cea.fr

UT-S&E-Tritium-Impact

Task Title: IMPACT OF CONTAMINATION WITH TRITIUM AT CELL LEVEL

INTRODUCTION

Ionizing radiation produces different kinds of damages among them oxidative stress and DNA double strand breaks (DSB). DSB are mainly repaired by Homologous recombination (HR) and non-homologous end-joining (NHEJ) processes. The impact of Tritium on DNA integrity directly derives from the deposited energy and not from any chemical poisoning since tritium only generates water. However association with another contaminant, which affects cell response, can produce synergistic effects. Moreover, it is also possible that tritium incorporation engages cells in a response that could be inappropriate for a concomitant associated stress.
Our project aimed to study the impact of contamination with Tritium on cell survival, cell cycle, mutagenesis, HR and NHEJ. Moreover our project will study the impact of Tritium contamination on the cell response to an additional independent and well controlled DSB.
In 2006, we evaluated the impact of sub-lethal doses of contamination by ^{3}H-thymidine on a single DNA double-strand breaks (DSB) targeted into a homologous recombination (HR) substrate in hamster CHO cells.

2006 ACTIVITIES

Cells were cultured in the presence of different specific activities of labeled thymidine. After 20 hours, when incorporation reached a plateau and over 95% of cells contained labeled nucleotides, radioactivity incorporated into the DNA was counted in trichloroacetic acid (TCA) precipitates. In parallel cultures, cell cycle analysis, viability (cloning efficiency), homologous recombination frequency were measured (figure 1).

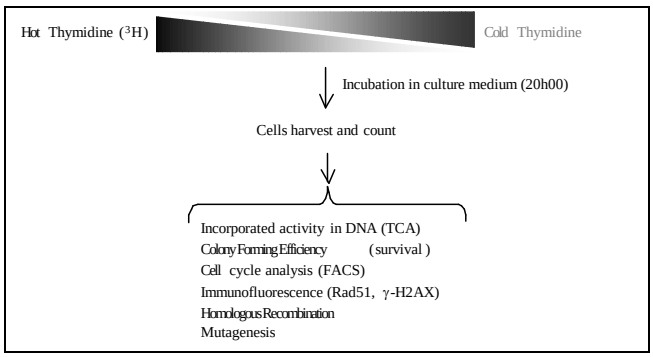

Figure 1

To analyze DSB-induced HR at a molecular and acute level, we measured HR induced by a specific DSB, targeted into the HR substrate (figure 2) by the meganuclease I-SceI, which strongly stimulates HR [4]. A HR event will repair the DSB induced by I-SceI and will restore a functional EGFP gene by gene conversion. EGFP positive cells will be scored by FACS analysis [1], [3]. A total of $3{\cdot}10^{5}$ cells were plated and transfected with 2 µg of the I-SceI expression vector (pCMV I-SceI).

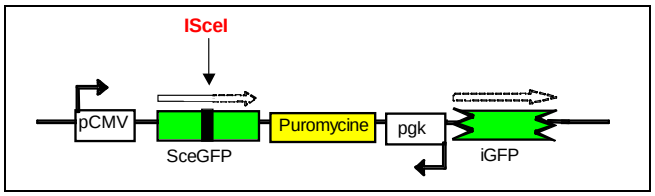

Figure 2

IMPACT OF 3H-NUCLEOTIDES CONTAMINATION ON THE CELL RESPONSE (SURVIVAL, CELL CYCLE, HR) TO AN ENZYMATIC DSB (I-SCEI)

Measure of survival

We incubate cells with ^{3}H-thymidine prior inducing DSB either by external gamma radiation (^{137}Cs irradiator, 40 DSB / nucleus / Gray) or by I-SceI expression (1 DSB / nucleus). Incorporation of ^{3}H-thymidine did not significantly affect toxicity induced by a single DSB produced by I-SceI expression. However, we found that incorporation of low doses of ^{3}H-thymidine before an external 6 Gy radiation increase cell survival. Moreover, incorporation of high doses of ^{3}H-thymidine does not increase cell survival after an external 6 Gy radiation. Taken together, these data show that a specific range of ^{3}H-thymidine incorporation may be able to activate cell protection pathways and then allow her to a better survival after a tougher secondary stress.

Measure of cell cycle

Cell cycle repartition was measured by regular methods. In 2005, we showed that there is no effect on the cell cycle repartition of ^{3}H-thymidine incorporation until $1{\cdot}10^{6}$ dpm/10^{6} cells. From that dose and upper, we measured a G2/M phase arrest mediated by the ATR signaling pathway. We found no effect on the cell cycle repartition of I-SceI induced DSB repair after ^{3}H-thymidine incorporation.

Homologous Recombination induction analysis

We incubate CHO-DRA10 or SV40-immortalized human fibroblasts RG37 cells with ^{3}H-thymidine prior inducing DSB either by external gamma radiation (^{137}Cs irradiator, 40 DSB / nucleus / Gray). We used the RG37 cells to measure the impact ^{3}H-thymidine incorporation on HR induced by I-SceI (1 DSB / nucleus). The presence of an I-SceI cleavage site allows the targeting of a specific

chromosomal double-strand cut, at a precise position in the HR substrate (figure 2). EGFP as reporter can be used to measure recombinant cells, instead of recombinant colonies with G418 resistance, and thus to measure HR independently of the fate of the recombinant cell.
Our results show that incubation with ^{3}H-thymidine prior to I-SceI transfection may reduce the percentage of recombinant cells (figure 3). The result may be explained by the hypothesis of an induction of the NHEJ pathway by ^{3}H-thymidine incorporation. The competition between both DSB repair pathways (HR and NHEJ) will be then turned in favor of NHEJ. We found a comparable decrease of RH repair of DSB induced by external gamma radiation after incorporation of low doses of ^{3}H-thymidine.
Incorporation of higher doses of ^{3}H-thymidine lead to HR stimulation as in control samples. This last result may not be easy to interpret in a robust model and shall need extra work before.

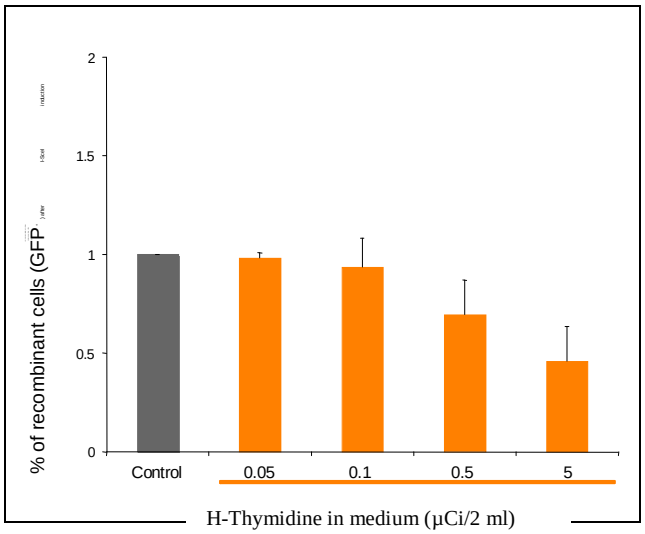

Figure 3

CONCLUSIONS

This part of our project shows some results that may be promising. We will need to perform extra investigations to clearly conclude to an effect of tritium contamination on a DSB induced by a subsequent genotoxic stress.

REFERENCES

[1] Dumay.A, Laulier C, Bertrand P, Saintigny Y, Lebrun F, Vayssiere JL, Lopez B. S. (2006). Bax and Bid, two proapoptotic Bcl-2 family members, inhibit homologous recombination , independently of apoptosis regulation. Oncogene. May 25;25(22):3196-205

[2] Lambert. S, and Lopez, B. S. (2000). Characterization of mammalian RAD51 double strand break repair using non lethal dominant negative forms. EMBO J 19, 3090-3099

[3] Pierce AJ, Jonhson RD, Thompson LH, Jasin M. (1999) XRCC3 promotes homology-directed repair of DNA damage in mammalian cells. Genes Dev. Oct 1513(20):2633-8

[4] Liang F, Han, M., Romanienko, P. J., and Jasin, M. (1998). Homology-directed repair is a major double-strand break repair pathway in mammalian cells. Proc Natl Acad Sci U.S.A. 95, 5172-5177.

REPORTS AND PUBLICATIONS

Roche S., Saintigny Y., Meynard D. and Lopez B. S. Non-toxic doses of 3H-thymidine or 14C-thymidine strongly stimulate RAD51-dependent recombination in mammalian cells. (to be submited)

Delacôte F., Deriano L., Lambert S., Bertrand P., Saintigny Y. and Lopez B. S. (2006) Chronic exposure to sub-lethal doses of radiation mimetic ZeocinTM selects for clones deficient in homologous recombination. Accepted in Mutation Research

Saintigny Y. Roche S., Meynard D. and Lopez B. S. Impact of contamination with tritium or radiocarbon at cell level. Environmental Mutagen Society 37th Annual Meeting, September 2006. Vancouver - Canada. Poster.

Saintigny Y. Impact of contamination with tritium at cell level. Plasticité et Instabilité des Génomes, 2nd Réunion Annuelle, November 2006. Grenoble - France

Saintigny Y. Impact of contamination with tritium or radiocarbon at cell level. Environmental Mutagen Society 37th Annual Meeting, September 2006. Vancouver - Canada

Saintigny Y. Interaction du tritium sur la réponse aux stress génotoxiques et la stabilité du génome. 4th annual seminar of French National Program of Nuclear Toxicology and Environment (ToxNuc-E), December 2006. Campus Michel-Ange du CNRS, Paris – France.

TASK LEADER

Yannick SAINTIGNY and Bernard S. LOPEZ

DSV/DRR/SRMC/LMR
CEA-Fontenay aux Roses
Boîte Postale 6
F- 92265 Fontenay aux Roses Cedex

Tel. : 33 1 46 54 88 35
Fax : 33 1 46 54 89 55

e-mail : bernard.lopez@cea.fr
yannick.saintigny@cea.fr